 doi:10.20944/preprints202201.0082.v1

Article

The cationic amphiphilic drug hexamethylene amiloride eradicates bulk breast cancer cells and therapy-resistant subpopulations with similar efficiencies

Anastasia L. Berg, Ashley Rowson-Hodel, Michelle Hu, Michael Keeling, Hao Wu, Kacey VanderVorst, Jenny J. Chen, Jason Hatakeyama, Joseph Jilek, Courtney A. Dreyer, Madelyn R. Wheeler, Ai-Ming Yu, Yuanpei Li, and Kermit L. Carraway, III*

[1] Department of Biochemistry and Molecular Medicine and University of California Davis Comprehensive Cancer Center, University of California Davis School of Medicine, Sacramento, CA, USA
* Correspondence: klcarraway@ucdavis.edu

Simple Summary: A limitation to successful therapeutic outcomes for breast and other cancer patients is the ability of small subsets of tumor cells to resist the apoptotic cell death provoked by currently employed therapeutic agents. These therapy-resistant cancer stem cell populations can then seed recurrent tumors and metastatic lesions, compromising the efficacy of the treatment regimen. The aim of our study was to assess the hypothesis that cationic amphiphilic drugs (CADs), which induce tumor cell death via the unrelated programmed necrotic mechanism, exhibit efficacy toward cancer stem cell populations that are resistant to currently employed therapeutics. We find that the therapy-resistant stem-like subpopulation of cells from a variety of breast cancer models are as sensitive to CADs as are the bulk population. Our observations imply that the incorporation of cationic amphiphilic anti-cancer agents into existing therapeutic regimens could ultimately improve breast cancer patient outcomes by minimizing tumor recurrence and metastatic outgrowth.

Abstract: The resistance of cancer cell subpopulations, including cancer stem cell (CSC) populations, to apoptosis-inducing chemotherapeutic agents is a key barrier to improved outcomes for cancer patients. The cationic amphiphilic drug hexamethylene amiloride (HMA) has been previously demonstrated to efficiently kill bulk breast cancer cells independent of tumor subtype or species, but acts poorly toward non-transformed cells derived from multiple tissues. Here we demonstrate that HMA is similarly cytotoxic toward breast CSC-related subpopulations that are resistant to conventional chemotherapeutic agents, but poorly cytotoxic toward normal mammary stem cells. HMA inhibits the sphere-forming capacity of FACS-sorted human and mouse mammary CSC-related cells *in vitro*, specifically kills tumor but not normal mammary organoids *ex vivo*, and inhibits metastatic outgrowth *in vivo*, consistent with CSC suppression. Moreover, HMA inhibits viability and sphere formation by lung, colon, pancreatic, brain, liver, prostate and bladder tumor cell lines, suggesting that its effects may be applicable to multiple malignancies. Mechanistically, HMA elicits the permeabilization of the limiting lysosomal membrane, a hallmark feature of the lysosome-dependent cell death pathway. Our observations expose a key vulnerability intrinsic to cancer stem cells, and point to novel strategies for the exploitation of cationic amphiphilic drugs in cancer treatment.

Keywords: breast cancer; cancer stem cell; therapy resistance; cationic amphiphilic drug; lysosome-dependent cell death

 doi:10.20944/preprints202201.0082.v1

1. Introduction

Studies in both hematological and solid tumor malignancies support the notion that tumor-initiating or cancer stem cells (CSCs) – a rare, relatively quiescent, and highly tumorigenic cancer cell population endowed with the capacity for self-renewal, anchorage independence, and multilineage differentiation – harbor intrinsic therapy resistance mechanisms and pose significant clinical challenges [1-5]. CSCs are resistant to cellular stresses [6], persist during therapeutic intervention [7], convey substantial tumor chemoresistance [8], potentiate post-therapy recurrence [9], and are strongly associated with progressive, metastatic disease [7].

While a potentially promising strategy, therapeutically targeting CSCs presents unique obstacles considering their notorious resistance to apoptotic death and capacity to launch primary tumor recurrence and metastases, even in cases of apparent complete clinical remission [3,10]. Insensitivity to caspase-dependent apoptotic signaling is among the most important factors conferring enhanced tumor growth, survival, and resistance to traditional chemotherapeutics and targeted drugs [11-13]. Accordingly, novel therapeutics that engage non-apoptotic cell death pathways to kill CSCs and other apoptosis-resistant tumor cells warrant investigation.

We have reported that 5-(*N*,*N*-hexamethylene) amiloride (HMA), a derivative of the FDA-approved potassium sparing diuretic amiloride and a member of the broader class of cationic amphiphilic drugs (CADs) [14-16], is cytotoxic toward cultured breast cancer cells independent of caspase activity [17]. HMA reduces the viability of breast cancer cells of differing molecular profiles with equal efficiency [17], which is significant as breast cancer subtypes (luminal or basal; estrogen/progesterone receptor positive [ER/PR+], HER2 amplified [HER2+], or receptor negative [ER/PR/HER2-]) are variably resistant to chemotherapeutics and targeted drugs [18]. Further, HMA is equally effective in eradicating both dividing and non-dividing cells [17], distinguishing it from cytotoxic agents that are employed clinically to kill actively proliferating cells but that can leave behind the quiescent CSC population responsible tumor repopulation. Clinical disease recurrence, in fact, is often observed following use of commonly employed anti-mitotic agents (i.e., taxanes, vinca alkaloids, kinase inhibitors, etc.) [19].

Fundamental to HMA's ability to deplete heterogeneous tumor cell populations is its capacity to induce a form of necrotic cell death initiated by disruption of lysosomal function and requiring lysosomal cathepsin activity for cell death [17], unlike commonly cited forms (e.g., necroptosis and parthanatos). HMA induces aggregation of acidic vesicles and formation of lysosomal multilamellar bodies, indicative of perturbed lysosomal membrane dynamics [17]. Indeed, lysosomes have been described as 'suicide-bags' based on the hydrolytic capacity of sequestered enzymes [20], and cell autolysis following lysosomal membrane permeabilization (LMP) has been shown to mediate cancer cell death [21-24]. Direct engagement of LMP leading to lysosome-dependent cell death (LDCD) has been demonstrated for a limited number of CADs and has been postulated as an attractive strategy for the eradication of apoptosis-resistant cancer cells [22,25]. Recent findings reveal that cancer cell lysosomes are particularly fragile, with heightened susceptibility to LMP [26]. Cells undergo characteristic morphological and functional changes during the process of malignant transformation, including alterations in lysosomal volume, quantity, membrane structure and composition, and hydrolase activity [20,24,26]. Paradoxically, these transformation-associated changes that promote tumor growth and invasiveness also render cancer cell lysosomes unstable and represent a cancer-specific vulnerability that might be exploited for therapeutic purposes. However, the sensitivity of the CSC population to CAD-induced LMP is currently unknown.

Here we establish the susceptibility of chemotherapy-insensitive cancer cells and CSC-related cells isolated from an array of tumor types to HMA-induced LDCD, leading to the novel suggestion that CADs may exhibit benefit as components of maintenance therapy following primary treatment.

Preprints (www.preprints.org) | NOT PEER-REVIEWED | Posted: 6 January 2022 doi:10.20944/preprints202201.0082.v1

2. Materials and Methods

2.1. Cell Culture

MDA-MB-231, MCF7, SKBR3, T47D, 4T1, nMuMG, T98G, Du145, A549, HepG2, J82, LS174T, Panc-1, and SKOV3 cells were purchased from American Type Culture Collection (ATCC, Manassas, VA, USA) and maintained as recommended at 37° in 10% CO_2 in media supplemented with 10% fetal bovine serum (FBS, Genesee Scientific) and antibiotics (penicillin/streptomycin; Gibco - Thermo Fisher). MCF10A (ATCC) cells were grown in DMEM/F12 (#SH30023, HyClone) base medium with growth factors. HMEC4 (gifted by K. Rao) cells were maintained in mammary epithelial basal media (MEBM; #CC-3151, Lonza) with MEGM SingleQuots Supplements (#CC-4136, Lonza). Met-1 (gifted by A.D. Borowsky) and NDL cells were maintained as previously described [27,28]. Cell lines were authenticated prior to use by short-tandem repeat profiling (Genetics Core Facility; University of Arizona, Tucson, AZ, USA) and were replaced with a cryopreserved stock every six passages. Mouse brain tissue was dissociated as described [29,30], and primary cells were cultured in DMEM base medium (#11995065, Gibco) for no more than one passage. Cell line attributes are summarized in Supplementary Tables S1 and S2.

2.2. Cell Viability Assays

Trypan blue staining was carried out as described previously [17] and counted using a Countess™ II Automated Cell Counter (Thermo Fisher). For MTT assays, media from treated cells was replaced with 5mg/mL 3-(4,5-Dimethyl-2-thiazolyl)-2,5-diphenyl-2H-tetrazolium bromide (MTT, #M5655, Sigma Aldrich) solution in base media for 1hr. Cells were washed with PBS, crystals were dissolved using isopropyl alcohol (IPA, 0.5% 1N HCl in isopropanol), and absorbance (λ_{ex} 570nm) was measured with a FilterMax F5 microplate reader (Molecular Devices) and Multi-Mode Analysis software (Version 3.4.0.27, Beckman Coulter).

2.3. Generation of MMTV-NDL mice

All experimental protocols were approved by the IACUC of the University of California, Davis, USA. The MMTV-NDL mouse model has previously been described [31]. Wild type females were crossed with NDL males to generate WT and NDL mice, and genotypes were confirmed by polymerase chain reaction using primers for NDL (Fwd-TTCCGGAACCCACATCAG; Rev-GTTTCCTGCAGCAGCCTA).

2.4. Cell Labeling, Flow Cytometry and Sorting

MDA-MB-231, MCF7 and SKBR3 human cancer cell lines were trypsinized to single cells, and MMTV-NDL murine mammary tumors (1.0-1.5 cm in diameter) were harvested and dissociated to single cells as previously described [29,30] with minor modifications. Cells were suspended at $1x10^7$ per mL in staining buffer (PBS with 2% FBS) and incubated for 30 minutes on ice with antibodies. Cells were washed three times, re-suspended in staining buffer with 1µg/mL Propidium Iodide (PI), analyzed, and sorted with a FACS Aria II cell sorter (Becton Dickinson). Sorting schemes were based on previously published studies for human cell lines [1,8] and primary mouse tissues [32,33]. Results were analyzed using FlowJo software. Antibodies used were CD24-PE-Cy7 (1:100 dilution, #561646, BD Pharmingen) and CD44-APC (1:100 dilution, #559942, BD Pharmingen) for human cells, and CD24-PE (1:200 dilution, #553262, BD Pharmingen), CD49f-APC (1:100 dilution, #313615, Biolegend), CD31-PE-Cy7 (1:100, #102417, Biolegend), and CD45-PE-Cy7 (1:100, #103113, Biolegend) for mouse cells.

2.5. Tumorsphere/Mammosphere Assays

For all sphere assays, single cells were plated at a density of $2\text{-}5x10^3$ cells per well on Corning Costar ultra-low attachment 24-well plates (#CLS3473, Sigma Aldrich), and spheres >50µm in diameter were quantified. FACS sorted cells from human cell lines were plated in serum-free MammoCult base medium with proliferation supplement (#05620,

Preprints (www.preprints.org) | NOT PEER-REVIEWED | Posted: 6 January 2022 doi:10.20944/preprints202201.0082.v1

Stem Cell Technologies), and sorted cells from murine mammary tumors were plated in DMEM/F12 medium containing basic fibroblast growth factor (bFGF, 20ng/mL, #354060, Corning), epidermal growth factor (EGF, 20ng/mL, #354001, Corning), heparin (4μg/mL, #07980, Stem Cell Technologies), and B-27 supplement (1:50 dilution, #17504044, Thermo Fisher). Cells were treated with vehicle (DMSO), HMA (#A9561, Sigma Aldrich), or chemotherapeutics (Cisplatin [#479306, Sigma Aldrich], Docetaxel [#S1148, Selleckchem], Doxorubicin [#S1208, Selleckchem]) prior to suspension.

For secondary sphere forming assays, cell lines were cultured to 70% confluency in two-dimension and treated with vehicle or HMA for 24 hours. Cells were then trypsinized to single cells and plated in ultra-low attachment plates as follows: MDA-MB-231, MCF7, SKBR3, and T47D in MammoCult medium; MCF10A, HMEC4, and nMuMG in MEGM; T98G, Du145, A549, HepG2, J82, LS174T, Panc-1, and SKOV3 in 3D Tumorsphere Medium XF (#C-28070, PromoCell). After 7 days, primary spheres were dissociated to single cells by trypsinization and re-plated in ultra-low attachment plates to grow for another 7 days. Secondary spheres were quantified.

For tumorsphere assays for chemoresistance, cell lines were cultured in two-dimensions and treated with chemotherapeutics as indicated for 72 hours. Single cell suspensions were plated at equivalent densities in ultra-low attachment plates in serum-free, MammoCult medium. A secondary dose of chemotherapeutic, HMA, or vehicle was then administered to cells in suspension, and tumorspheres were allowed to form over 7 days and then quantified. All images were captured using an Olympus IX81 inverted microscope and CellSens Entry software.

2.6. Persister Cell Generation and Treatments

An MCF7-persister cell population was generated based on previous studies [34,35]. Parental MCF7 cells were seeded in 12-well plates and cultured to 70-80% confluency prior to treatment with 4μM DTX. Cells were washed twice with PBS, and media with new drug was replaced every three days over a nine-day incubation period. MCF7 parental cells from the same persister line origin population were simultaneously cultured and plated on day 9 of persister line culture in 12-well plates, and both parental and persister cells were treated the next day with either vehicle control (DMSO), 4μM DTX, or 40μM HMA for 24 hours. Cell death was evaluated by trypan blue assay.

2.7. Ex Vivo *Organoid Assay for Drug Cytotoxicity*

MMTV-PyMT and MMTV-NDL murine mammary tumors (1.0-1.5 cm in diameter) or pooled mammary glands from FVB-NJ mice were harvested and dissociated to single cells as previously described [29,30] with minor modifications. $2x10^5$ single cells were embedded in Matrigel (#354230, Corning) in organoid growth medium on 24-well plates, which has been previously described [36]. Organoids were formed after 7 days in culture, and were then exposed to vehicle and varying concentrations of HMA for 72 hours. MMTV-PyMT and MMTV-NDL organoid viability was measured using RealTime Glo (#G9711, Promega) according to manufacturer's instructions. Images were taken before (Day 0) drug treatment and daily over the course of drug treatment. Representative brightfield images were taken with an Olympus IX81 microscope with CellSens Entry software; chemiluminescent images were taken with a ChemiDoc MP Imaging System (BioRad) and analyzed with Image Lab software to quantify RealTime Glo signal.

2.8. Establishment of Orthotopic Xenograft Mouse Models

All animal studies were performed in accordance with protocols approved by the Institutional Animal Care and Use Committee of the University of California, Davis. 8-12 week old Balb/cJ (#000651) and FVB/NJ (#001800) mice were purchased from The Jackson Laboratory and allowed to acclimate for at least one week before use. Orthotopic mammary fat pad implantation was performed as follows: $1\text{-}2x10^6$ syngeneic tumor cells (4T1 cells into Balb/cJ, Met-1 cells into FVB/NJ) suspended in PBS were mixed in a 1:1 volume/volume mixture of PuraMatrix Peptide Hydrogel (#354250, Corning) and injected

Preprints (www.preprints.org) | NOT PEER-REVIEWED | Posted: 6 January 2022 doi:10.20944/preprints202201.0082.v1

into the fourth mammary fat pads of mice under anesthesia by continuous inhalation of 2% isoflurane gas. Sterile tweezers were used to lift the fourth nipple, and a syringe needle was used to implant cell suspensions directly into the mammary fat pad. Tumors were measured twice weekly using digital calipers, and mice were sacrificed when tumors reached 1.0-1.5 cm in diameter.

2.9. Organotypic Tumor Slice Preparation and Viability Analysis

Cores 4mm in diameter were punched from sacrificed murine tumors using a biopsy punch (#7424, RoyalTek) and cut into 1mm organotypic tumor slices. Tumor slices were cultured individually on 12mm Transwell with 0.4μm pore polycarbonate membrane inserts (#3401, Corning) using 12 well plates. Slices were cultured in 1x Advanced Dulbecco's Modified Eagle Medium (#12491023, Thermo Fisher) supplemented with 5% FBS, 1x GlutaMAX (#35050061, Thermo Fisher), 0.5x Penicillin-Streptomycin, 1x Insulin-Transferrin-Selenium supplement (#41400045, Thermo Fisher), and 15mM HEPES (#15630130, Thermo Fisher) as previously described [37] and maintained at 37° in 10% CO_2. After 24 hours in culture, slices were exposed to vehicle or 40μM HMA for 24 hours. Tumor slice viability was measured using RealTime Glo (#G9711, Promega) according to manufacturer's instructions. Images were taken before (Day 0) drug treatment and 24 hours after drug treatment with a ChemiDoc MP Imaging System (BioRad) and analyzed with Image Lab software to quantify RealTime Glo signal.

2.10. Animal Therapeutic Studies

7-10 week old female FVB/NJ (#001800) mice were purchased from The Jackson Laboratory and allowed to acclimate for at least one week before use. For evaluation of intratumoral drug delivery, $3x10^6$ syngeneic Met-1 cells in PBS were mixed in a 1:1 volume/volume mixture of PuraMatrix Peptide Hydrogel (#354250, Corning) and injected bilaterally into the fourth mammary fat pads of mice under anesthesia by continuous inhalation of 2% isoflurane gas. Sterile tweezers were used to lift the fourth nipple, and a syringe needle was used to implant cell suspensions directly into the mammary fat pad. Tumors were measured daily using digital calipers, and tumor volume was calculated according to the formula $v = (w^2 \times l) \times 0.5236$. When tumors reached a volume of $100mm^3$, animals were randomized into two cohorts (n=3) and unilaterally administered 0.78μg HMA per mm^3 tumor in 10% DMSO in saline or DMSO-saline control daily for 7 days. Contralateral tumors were un-injected and served as internal controls. Animals were sacrificed 2 days following treatment end by CO_2 asphyxiation; all tumors were collected and fixed in 10% neutral buffered formalin for paraffin embedding and sectioning, while lungs were fixed for whole-mount analysis.

For the experimental model of metastasis, $1x10^6$ NDL tumor cells in PBS were injected into the lateral tail vein of female FVB/NJ mice. After 7 days, randomized animals were treated intravenously with either HMA (30mg/kg)-loaded disulfide cross-linked micelles (DCMs) or empty DCMs twice weekly for four weeks. Polymer synthesis, micelle preparation, drug loading, and micelle size and distribution characterization for *in vivo* delivery were carried out as previously described [38]. Animals were sacrificed 24 hours after the final treatment, and tissues were harvested for analysis of metastasis. All mice were caged as mixed treatment cohorts.

2.11. Lung Analysis

Lungs were inflated with PBS, fixed in formalin for 24 hours at 4°C, and stained in carmine alum as described [39,40]. Gross lesions were imaged under a dissecting scope (Zeiss Stemi 2000-C; Axiocam ERc/5 s) and processed for confirmation by histology.

2.12. Histology

All drug-injected and un-injected contralateral control xenograft tumors were subjected to histological analysis. H&E-stained sections were prepared using previously described methods [39] and analyzed for presence of necrosis in a blinded fashion. Area of

Preprints (www.preprints.org) | NOT PEER-REVIEWED | Posted: 6 January 2022 doi:10.20944/preprints202201.0082.v1

active necrosis was quantified and normalized to total tumor area for 3-5 randomly selected fields across 3 serial sections. Immunohistochemistry was performed as previously described [41]. An internal negative control (no primary antibody) was included with each analysis.

2.13. Lysosomal Sequestration Assay

MDA-MB-231 and MCF7 wells were cultured on 96-well plates and treated with 50nM LysoTracker Red DND-99 (#L7528, Thermo Fisher) in combination with varying concentrations of HMA for 30 minutes. Cells were washed twice with PBS and solubilized with 100µl acetonitrile as described [42]. Samples were then analyzed for LysoTracker Red fluorescence (λ_{ex} 530nm, λ_{em} 590nm) with a FilterMax F5 microplate reader (Molecular Devices) and Multi-Mode Analysis software (Version 3.4.0.27, Beckman Coulter).

2.14. Lysosomal Stability Assays

For the dextran release assay, MDA-MB-231 and MCF7 wells were seeded on black/clear bottom 96-well glass microtiter plates (P96-1.5H-N, Cellvis) and incubated with 100µg/mL dextran Alexa Fluor™ 546 (10,000 MW, #D22911, Thermo Fisher) for 24 hours. After dextran loading, cells were washed twice with PBS, chased for 30 minutes in fresh medium, and treated with vehicle, 40µM HMA, 8µM Siramesine (#SML0976, Sigma Aldrich), 5µM Terfenadine (#T9652, Sigma Aldrich), and 2mM L-leucyl-L-leucine-methyl ester (LLOMe, # L1002, Sigma Aldrich) for 20 hours based on published studies [20,24]. Cells were washed twice with PBS and imaged with an Olympus IX81 inverted microscope and CellSens Entry software. Cells with dextran diffusion were quantified in five replicate fields with ImageJ software (NIH; http://rsb.info.nih.gov/ij/) and normalized to total cell count.

For the galectin translocation assay, MCF7 cells were plated on glass coverslips in 12 well plates and cultured to 70-80% confluency. Cells were treated with vehicle (DMSO), 2mM LLOMe, 8µM siramesine, or 40µM for 12 hours and then fixed with 4% paraformaldehyde for 10min. After fixation, translocation of galectin-3 to ruptured lysosomes was evaluated by immunocytochemistry as described [20]. Samples were incubated with 50mM ammonium chloride in PBS for 10min, washed three times with PBS, and then permeabilized and blocked in 1 mL blocking buffer (1% BSA, 0.02% sodium azide, 0.2% NP-40, 5% goat serum) at room temperature for 1hr. Cells were incubated with purified mouse anti-human Galectin-3 (1:100 dilution, #556904, BD Biosciences) diluted in blocking buffer for 1hr at room temperature. Cells were washed three times with PBS and then incubated with goat anti-mouse IgG1 cross-absorbed secondary antibody Alexa Fluor 488 (1:1,000 dilution, #A-21121, Invitrogen) at room temperature for 1hr. Cells were again washed three times with PBS before incubation with DAPI (1:10,000) in PBS for 10min in the dark and then rinsed twice with PBS twice before mounting with Fluoromount G. Slides were imaged by confocal microscopy using a ZEISS LSM 800 with Airyscan, and galectin-3 puncta formation was analyzed from five replicate fields with FIJI (https://imagej.net/Fiji) software.

2.15. Statistical, data, and image analysis

Values are expressed as averages and were calculated from a minimum of three replicate experiments, unless otherwise stated. Statistical significance was established using a student's t-test or Wilcoxon rank-sum test, with p-values less than 0.05 considered statistically significant. Data analysis and graphical representation were performed with Microsoft Excel or R-statistical platform. Images were compiled in Microsoft PowerPoint, with brightness and contrast altered only for presentation clarity.

3. Results

3.1. HMA ablates chemotherapy-resistant BCSCs but not normal mammary stem-like cells

Our previous studies demonstrated that HMA kills human- and mouse-derived mammary carcinoma cells, but not non-transformed cells from a variety of tissues,

Preprints (www.preprints.org) | NOT PEER-REVIEWED | Posted: 6 January 2022 doi:10.20944/preprints202201.0082.v1

independent of proliferative state or molecular subtype [17]. These observations raise the possibility that HMA may be cytotoxic toward the relatively quiescent CSC population, and that HMA treatment may circumvent the chemotherapeutic resistance characteristic of breast cancer subtypes [18]. For example, receptor-negative breast carcinomas are enriched for a CSC phenotype [43] and display increased recurrence and chemoresistance rates relative to luminal breast cancers [18], yet we observed that analogous cultured cell models (MDA-MB-231 and MCF7, respectively) respond similarly to HMA [17].

To assess the ability of HMA to specifically eradicate breast CSCs (BCSCs), we first examined the impact of HMA pretreatment on secondary sphere formation [44-46] by cultured human breast cancer cell lines. We observed that the EC_{50}s for HMA-mediated tumorsphere suppression toward bulk populations of MDA-MB-231 (ER/PR/HER2-), MCF7 and T47D (ER/PR+), and SKBR3 (HER2+) human breast cancer cell lines (see Supplementary Table S1) are essentially identical to each other (Fig. 1A) and identical to the EC_{50}s we previously reported for HMA cytotoxicity toward the total populations of these cell lines [17]. Likewise, $CD44^+/CD24^{low}$ sorted (see Supplementary Fig. S1A) MDA-MB-231, MCF7, and SKBR3 BCSC-enriched subpopulations are similarly sensitive to HMA (Fig. 1B). In contrast, EC_{50} levels of HMA did not reduce secondary sphere formation by the non-tumorigenic mammary epithelial human breast MCF10A and HMEC and mouse mammary nMuMG cell lines (Fig. 1C). These observations confirm the hypothesis that HMA is similarly cytotoxic toward BCSC subpopulations as bulk populations, and point to the existence of a therapeutic window that could circumvent a substantial barrier to CSC-targeted therapeutics development [47].

To discern whether therapy-resistant BCSC subpopulations are sensitive to HMA, we examined the sphere-forming capabilities of sorted cells after treatment with HMA or the apoptosis-inducing conventional chemotherapeutic agents cisplatin (CIS), or docetaxel (DTX) together with doxorubicin (DOX), at levels similar to their EC_{50}s for cytotoxicity toward the total cell population (Fig. 1D). We observed that while the $CD44^+/CD24^{low}$ subpopulations are resistant to these chemotherapeutic agents, they remain sensitive to HMA (Figs. 1E and Supplementary Fig. S1B). Given the inherent chemoresistance of BCSCs and their propensity to expand under selective pressures imparted by chemotherapy drugs [8], it was unsurprising that both CIS and combination DTX/DOX treatment exhibited enhanced sphere formation relative to vehicle control.

We observed similar effects of HMA on sphere outgrowth of BCSCs derived from mammary tumors arising in the MMTV-NDL transgenic mouse model of HER2-positive breast cancer. These mice develop metastatic multifocal adenocarcinomas at approximately 20 weeks of age [48,49]. The BCSC subpopulation was isolated by sorting (Supplementary Fig. S1C) for markers CD24 and CD49f [33] and lack of lineage-specific markers ($Lin^-/CD31^-/CD45^-$) [29,32,33]. The HMA EC_{50} for inhibition of mouse mammary tumorsphere outgrowth by sorted cells was comparable to that observed for human breast cancer cell lines (Fig. 1F), and HMA dramatically reduced sphere growth when compared to chemotherapeutics CIS and DTX/DOX (Fig. 1G and Supplementary Fig. S1B).

Preprints (www.preprints.org) | NOT PEER-REVIEWED | Posted: 6 January 2022 doi:10.20944/preprints202201.0082.v1

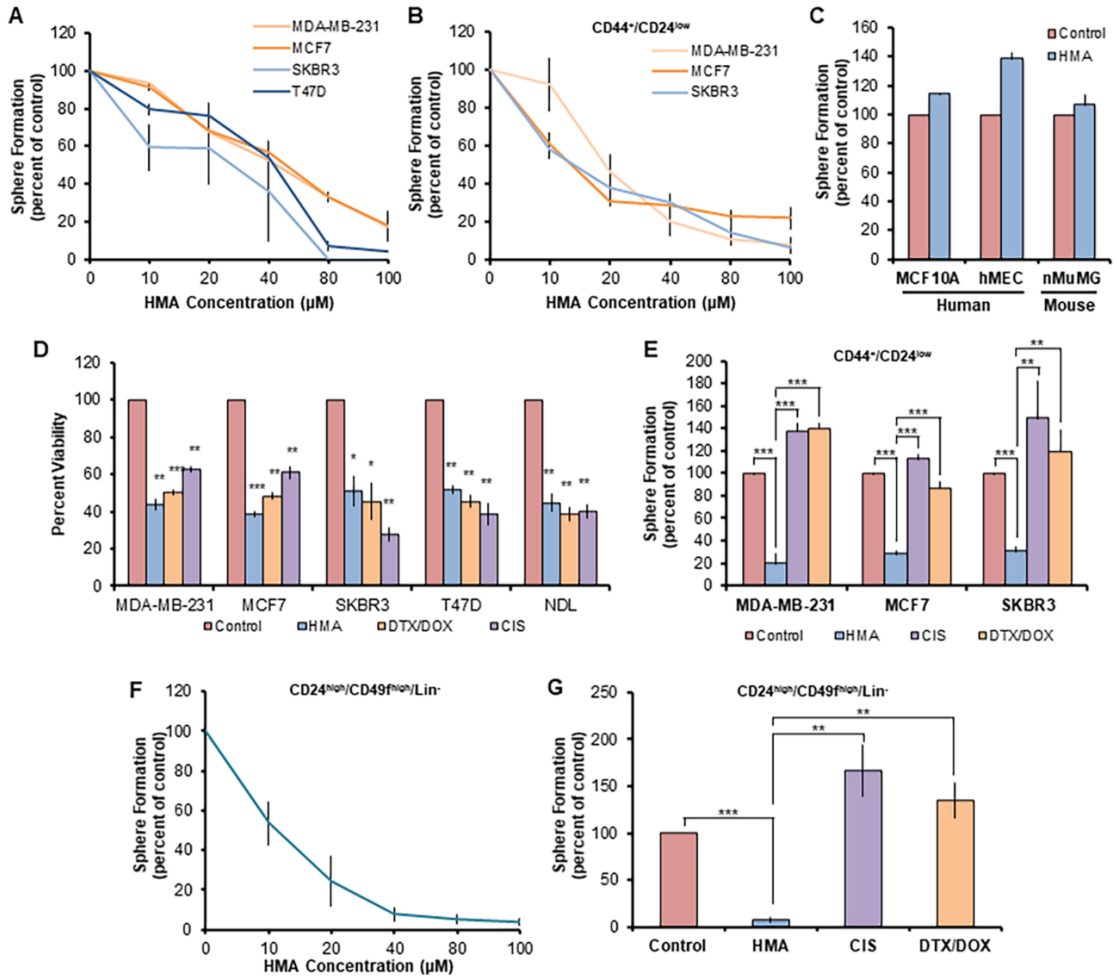

Figure 1. HMA ablates chemotherapy-resistant BCSCs but not normal mammary stem-like cells. **(A)** Secondary tumorsphere formation by human breast cancer cell lines was assessed after pretreatment with various concentrations of HMA for 24 hours. Data are representative of three independent experiments. **(B)** Secondary sphere formation by $CD44^{+}/CD24^{low}$ BCSC-enriched human breast cancer cells after HMA pretreatment. **(C)** Secondary mammosphere formation of non-transformed human and mouse mammary epithelial cell lines was assessed after 40μM HMA treatment for 24 hours. **(D)** Total populations of MDA-MB-231, MCF7, SKBR3, and T47D cells were treated with vehicle (DMSO), 40μM HMA, 40μM cisplatin (CIS), or a combination of 170nM doxorubicin (DOX) and 50nM docetaxel (DTX) for 24 hours, and cell viability was determined by trypan blue exclusion assay. **(E)** Sorted human BCSC cells were treated with vehicle, 40μM HMA, 40μM CIS, or 170nM DOX with 50nM DTX, and secondary sphere formation was determined. **(F,G)** Cells dissociated from MMTV-NDL mouse mammary tumors were sorted ($CD24^{high}/CD49f^{high}/Lin^{-}$) to enrich for the BCSC population, and 7-day sphere formation following pretreatment with HMA **(F)** or standard chemotherapeutics **(G)** was quantified over four biological tumor replicates from independent mice. Error bars represent SEM. *, $P < 0.05$; **, $P < 0.01$; ***, $P < 0.001$, by Student's t-test.

3.2. HMA is cytotoxic toward tumor cell populations insensitive to conventional chemotherapeutics

To directly assess HMA's ability to ameliorate chemotherapy resistance, we analyzed the chemotherapy-insensitive 'persister' cell population that survives cytotoxic Persister cells derived from the parental MCF7 line were generated through continuous 9-day culture in the presence of high-dose DTX (Supplementary Fig. S2A) and displayed insensitivity toward further DTX administration, but exhibited sensitivity to HMA to a degree comparable to that observed in the MCF7 parental cell line (Fig. 2A). Similarly, Met-1 mouse mammary carcinoma cells treated with high-dose CIS (Supplementary Fig. S2B) or DTX (Supplementary Fig. S2C) for 48 hours demonstrated therapy insensitivity upon secondary CIS or DTX treatment but were sensitive to HMA. Furthermore, when DTX-resistant cells

Preprints (www.preprints.org) | NOT PEER-REVIEWED | Posted: 6 January 2022 doi:10.20944/preprints202201.0082.v1

were plated in a tumorsphere assay following secondary DTX, HMA, or vehicle control administration, a significant reduction in sphere outgrowth from HMA-treated cells was observed, while sphere count was equivalent between secondary DTX- and control-treated cells (Supplementary Fig. S2D).

We further interrogated the capacity of HMA to target therapy-resistant human BCSCs by selecting for the BCSC subset in sphere-forming conditions following extended dosing with chemotherapy drugs. MDA-MB-231, MCF7, SKBR3, and T47D cell lines were cultured in the presence of DTX (Fig. 2B), CIS (Fig. 2C), or combination DTX/DOX (Fig. 2D) for 72 hours and subsequently plated in a tumorsphere assay. Secondary treatment with HMA yielded dramatic reduction in sphere formation, while treatment with chemotherapies consistently enriched for a BCSC phenotype. These observations affirm the potential of HMA to overcome both single- and multi-drug resistance uniformly across a variety of breast cancer subtypes.

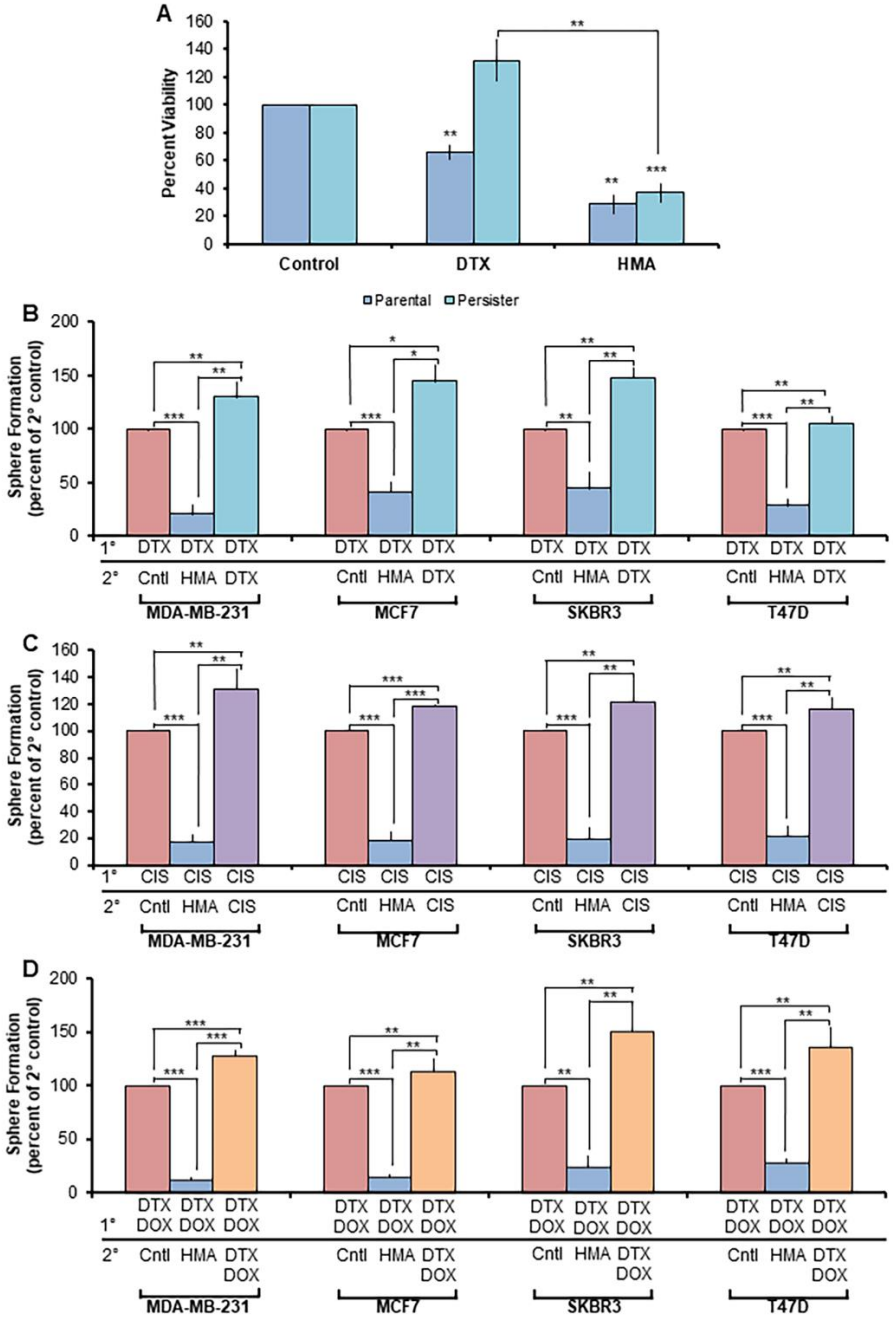

Figure 2. HMA is cytotoxic toward tumor cell populations insensitive to conventional chemotherapeutics. (A) Parental and DTX-persister cells were treated with vehicle, 4μM DTX, or 40μM HMA for 24 hours, and trypan blue exclusion assay was used to assess cell viability. Data are representative

 doi:10.20944/preprints202201.0082.v1

of five biological replicate experiments. **(B-D)** Breast cancer cell lines were treated with primary (1°) chemotherapy treatments – **(B)** 100nM DTX, **(C)** 40μM CIS, and **(D)** 170nM DOX/50nM DTX – for 72 hours and then plated in serum-free, low adherent conditions to enrich for the chemotherapy-insensitive BCSC population. Cells were subsequently treated with vehicle, 40μM HMA, or a secondary (2°) chemotherapeutic treatment. Average sphere count was assessed after 7 days. Data are representative of three independent studies. Error bars represent SEM. *, $P < 0.05$; **, $P < 0.01$; ***, $P < 0.001$, by Student's t-test.

3.3. HMA thwarts the viability of mouse mammary tumor tissues ex vivo

To evaluate HMA efficacy in more physiological relevant systems recapitulating complexities of the *in vivo* environment, we adapted an *ex vivo* primary tumor organoid model [36] to incorporate fundamental properties of tissue architecture using the MMTV-NDL and MMTV-PyMT transgenic mouse models of breast cancer [48,51]. Fresh tumor tissues were dissociated to single cells and embedded in a 3-dimensional Matrigel scaffold for 7-day culture to produce tumor organoids. Organoid viability over the course of subsequent 72-hour HMA treatment was monitored in real time with the use of a non-lytic, bioluminescent method. We observed that HMA dramatically reduces both MMTV-PyMT (Fig. 3A) and MMTV-NDL (Fig. 3B) organoid viability over time, which can be distinguished by a dramatic change in organoid morphology and loss of structural integrity by bright field imaging (Figs. 3C and 3D). In contrast to the marked reduction in tumor-derived organoid viability observed in response to HMA (Fig. 3D, *left panels*), viability and morphology of organoids generated from matched normal FVB/NJ mouse mammary gland were unaffected by HMA treatment over 48 hours (Fig. 3D, *right panels*).

Recently, a novel organotypic tumor slice culture method was developed to interrogate the tumor immune microenvironment and cancer cell response to cytotoxic agents in the context of a heterogeneous tissue retaining complex tumor architecture [52]. Cores are punched from fresh tumor tissues and then sliced for individual *ex vivo* culture on transwell inserts. We employed this technique to assess HMA impact on several mouse mammary tumor models, including the MMTV-NDL and MMTV-PyMT transgenic mouse models as well as two orthotopic syngeneic mammary xenograft models of aggressive disease (BALB/cJ and FVB/NJ mice transplanted with 4T1 and Met-1 mouse mammary tumor cells, respectively). Slice viability was verified by bioluminescence prior to drug administration and evaluated after 24 hours of HMA treatment, revealing striking loss of viability signal (Fig. 3E) and marked tumor cytotoxicity across all four models (Fig. 3F).

Preprints (www.preprints.org) | NOT PEER-REVIEWED | Posted: 6 January 2022 doi:10.20944/preprints202201.0082.v1

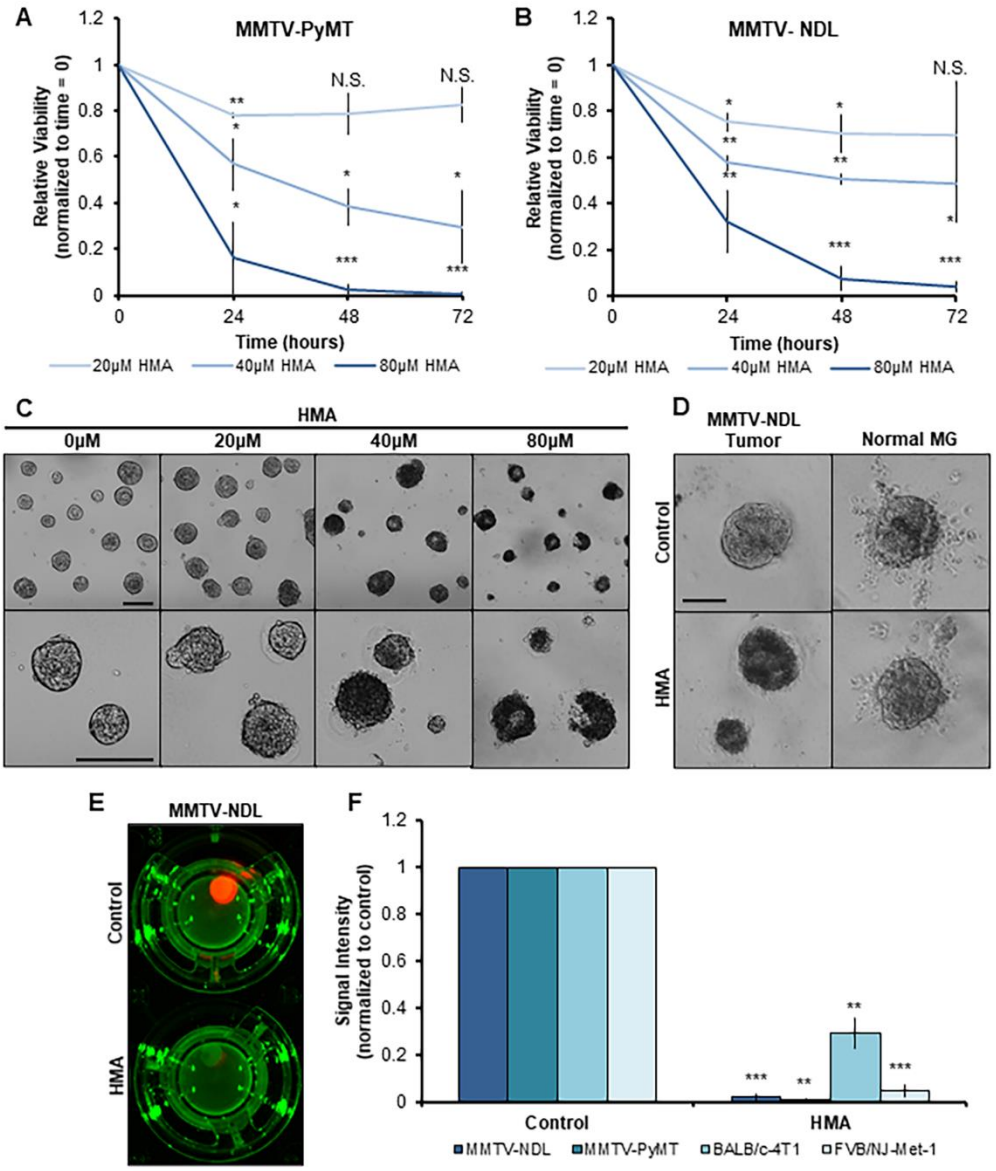

Figure 3. HMA impacts viability of mouse mammary tumor tissues *ex vivo*. (A-D) Organoids dissociated from MMTV-PyMT **(A, C)** or MMTV-NDL **(B, D)** mouse mammary tumors were administered increasing concentrations of HMA for 72 hours. **(A-B)** RealTime Glo viability signal intensity was measured every 24 hours and normalized to pre-treatment organoid viability (time = 0) and vehicle control. Data encompasses three biological tumor replicates from independent mice. **(C)** Representative images of MMTV-PyMT organoids following 72-hour treatment are displayed. Scale bar = 200μm. **(D)** Organoids derived from MMTV-NDL tumor (left) and normal mammary gland (right) were treated with 40μM HMA or vehicle control for 48 hours, and representative images are presented. Scale bar = 50μm. **(E, F)** Tumor tissue slices from genetically modified mouse models of mammary tumorigenesis (MMTV-NDL, MMTV-PyMT) and orthotopic mammary xenograft models (BALB/cJ-4T1, FVB/NJ-Met-1) were exposed to vehicle (DMSO) and 40μM HMA for 24 hours, and overall tumor tissue viability was assessed by RealTime Glo exposure. **(E)** Representative images of luminescent viability signal measured in control and HMA-treated MMTV-NDL tumor slices are shown. **(F)** Quantification of signal intensity indicating tissue viability over three to six tumor replicates from independent mice is shown. Signal was normalized to the intensity of each slice at time = 0, and then to vehicle control. Error bars represent SEM. *, $P < 0.05$; **, $P < 0.01$; ***, $P < 0.001$, by Student's t-test.

 doi:10.20944/preprints202201.0082.v1

3.4. HMA induces necrosis in vivo and suppresses metastasis

We previously demonstrated that HMA induces the programmed necrotic death of cultured cancer cells by a lysosome-dependent mechanism [17]. To affirm that HMA invokes a comparable mode of cytotoxicity *in vivo*, we generated a syngeneic xenograft model of mammary tumorigenesis via transplantation of Met-1 mouse mammary carcinoma cells directly into the mammary glands of FVB/NJ mice. We observed that daily direct intratumoral injection of HMA for 7 days results in a significant increase in necrotic tumor area by histology relative to vehicle control treated tumors as well as un-injected contralateral control tumors (Figs. 4A and 4B). The modest necrosis observed in the vehicle control tumors may be accounted for by injection force shear. Met-1 cells are highly aggressive and readily metastasize to the lung, and notably, gross morphological and histological analysis of lung tissues collected from HMA-treated animals revealed fewer metastatic lesions than those from vehicle control-treated animals (Figs. 4C and 4D). These findings are consistent with a reduced capacity for BCSCs to survive and establish metastatic foci following necrotic death induced by HMA.

We next sought to investigate whether HMA impacts metastatic colonization of tumor cells when injected directly into the vasculature. We established an experimental model of metastasis whereby NDL mouse mammary tumor cells were instilled into the lateral tail vein of FVB/NJ mice [39]. Systemic delivery of the naked HMA compound has little impact on overall tumor burden (not shown) due to its short half-life *in vivo* [53,54]. To enhance drug bioavailability for these studies, we encapsulated HMA in reversibly disulfide cross-linked micelles (DCMs) that minimize premature drug release in circulation. HMA-loaded (5mg/mL) DCM nanoparticles were determined to have uniform size by dynamic light scattering methods [38], indicating sufficiency for *in vivo* delivery (Supplementary Fig. S3A), and exhibited equivalent cytotoxicity to free drug S3B). Beginning 7 days after cell instillation, animals were treated intravenously with 30mg/kg HMA/DCM or empty DCM control twice weekly for four weeks, and harvested lung tissues were analyzed by gross morphology and histology (Fig. 4E). We observed a significant reduction in metastatic lung colonization with systemic HMA/DCM treatment relative to DCM control (Fig. 4F). Animal body weights were stable during systemic treatment, indicating a lack of drug toxicity (Supplementary Fig. S3C). These observations affirm that HMA effectively inhibits tumor metastasis and secondary tumor initiation at distant tissue sites in animal models of breast cancer, again consistent with its ability to eradicate the BCSC subpopulation.

Preprints (www.preprints.org) | NOT PEER-REVIEWED | Posted: 6 January 2022 doi:10.20944/preprints202201.0082.v1

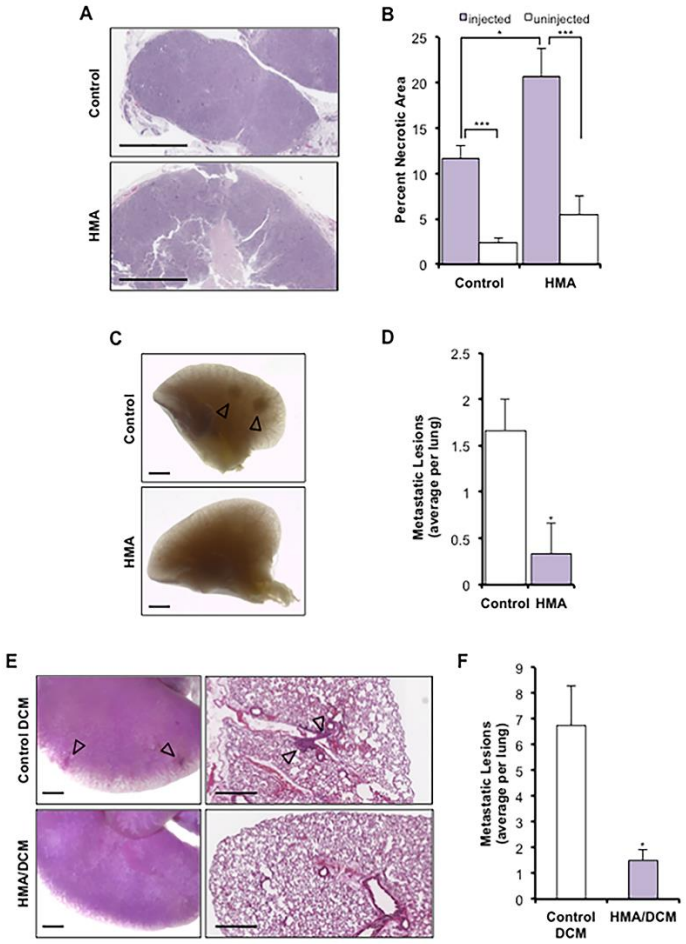

Figure 4. HMA induces necrosis *in vivo* and suppresses metastasis to the lung. (A-D) Met-1 xenograft mammary tumors received daily intratumoral injection of HMA (0.78μg/mm^3 tumor volume) or vehicle for 7 days (n = 3 FVB/NJ mice per cohort). **(A)** Representative H&E-stained sections; scale bar = 1mm. **(B)** Necrotic area is presented as a percentage of total tumor area (mean ± SEM) and compared to uninjected contralateral (internal animal control) tumors. Significance was determined by Student's t-test. **(C)** Carmine alum-stained lung tissue was evaluated for the occurrence of gross lesions (arrows); scale bar = 1mm. **(D)** The numbers of gross metastatic lesions per mouse (mean ± SEM) are depicted for each treatment cohort, and significance was determined by Student's t-test. **(E,F)** NDL tumor cells were instilled into the lateral tail vein of FVB/NJ mice, and animals were treated intravenously twice weekly for four weeks with HMA (30mg/kg)-loaded DCMs (HMA loading: 5mg/mL) or empty DCM (n = 4 mice per cohort). **(E)** Metastatic colonization of the lungs was determined by carmine alum staining; scale bar = 1mm. **(F)** Quantification of metastatic lung lesions per animal (mean ± SEM). Significance was determined by Wilcoxon rank-sum test with continuity correction. *, $P < 0.05$; **, $P < 0.01$; ***, $P < 0.001$ for all panels.

3.5. HMA depletes cancer cells derived from an array of human tissue types and inhibits outgrowth of enriched cancer stem-like populations

Considering the remarkable consistency of HMA's cytotoxic effects in diverse breast cancer cell lines and tissues as described here and in our previous report [17], we investigated whether HMA might be utilized as a pan-therapeutic for malignancies arising from other tissues. To address this question, we tested the impact of HMA on transformed human cell lines derived from an array of solid tissue tumor types (Supplementary Table S2). T98G, Du145, A549, HepG2, J82, LS174T, Panc-1, and SKOV3 cell lines all demonstrated a dose-dependent response to HMA (Fig. 5A) and exhibited EC_{50} values very similar to bulk breast cancer cell lines and BCSCs. Notably, HMA is cytotoxic toward T98G cells derived from glioblastoma, an aggressive form of brain cancer with poor clinical prognosis due to a distinct lack of therapeutic options [55,56], but not toward cells dissociated from fresh mouse brain tissue (Fig. 5B).

Preprints (www.preprints.org) | NOT PEER-REVIEWED | Posted: 6 January 2022 doi:10.20944/preprints202201.0082.v1

We further examined HMA's effects on non-breast CSCs using the tumorsphere assay. Low-adherent growth conditions enrich for the CSC population across cell types [57,58], and all cell lines tested displayed a statistically significant reduction in secondary sphere outgrowth following 24-hour EC_{50} HMA treatment with the exception of LS174T and Du145, which fell outside of significance because of the inherent variability in sphere formation across multiple biological replicates (Figs. 5C and 5D). The highly aggressive and therapy-resistant lines T98G [59], Panc-1 [60], A549 [61], and HEPG2 [62] exhibited marked reduction in secondary sphere formation in response to HMA compared to control. Notably, we observed elevated levels of cellular debris in the HMA-treated samples, which in combination with reduced sphere number indicated increased cellular stress and CSC death. The striking CSC morbidity reflected in the impaired sphere outgrowth observed across cell lines representing diverse solid tumor types underscores the potentially broad therapeutic applications of HMA mechanism of action in cancer treatment.

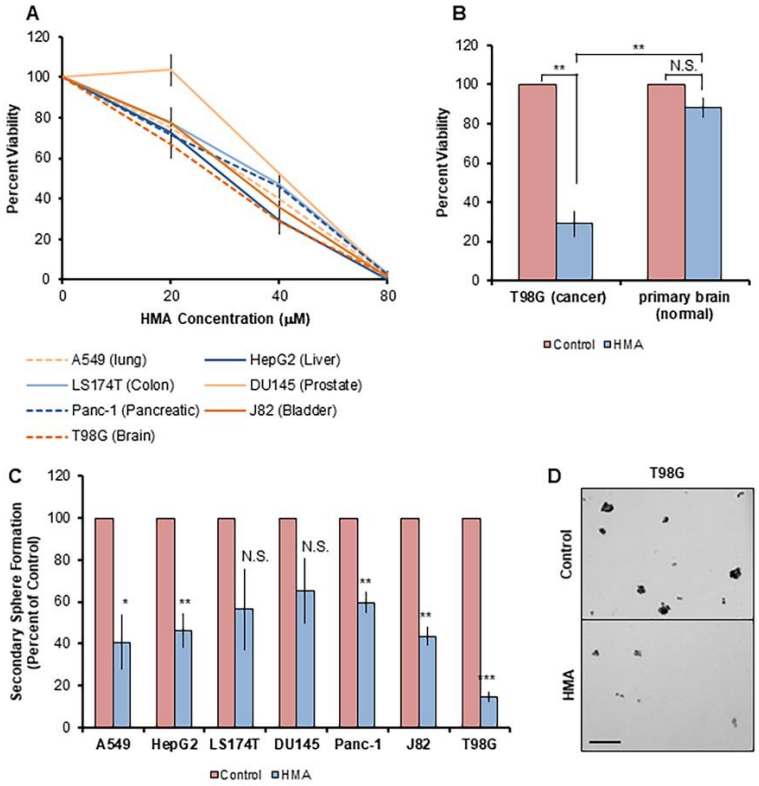

Figure 5. HMA depletes CSCs derived from an array of human tissue types. (A) The viability of human tumor cell lines treated with varying concentrations of HMA for 24 hours was assessed by trypan blue exclusion assay. Data are presented as averages of at least three independent biological trials and expressed as a percent of vehicle control. **(B)** T98G glioblastoma cells and nontransformed mouse primary brain glial cells were subjected to 24 hour treatment with 40μM HMA. Cell viability representative of three replicate trials is normalized to vehicle control. **(C)** Cell lines were treated with vehicle or 40μM HMA for 24 hours and then subjected to the sphere formation assay. Secondary sphere formation is presented as average sphere count of at least three independent biological experiments and normalized to vehicle control. **(D)** Representative images of DMSO control and 40μM HMA treated T98G spheres are displayed. Scale bar = 200μm. Error bars represent SEM. *, $P < 0.05$; **, $P < 0.01$; ***, $P < 0.001$, by Student's t-test.

3.6. HMA induces lysosomal membrane permeabilization

We previously established that HMA engages a caspase-independent mode of necrotic cell death requiring lysosomal cathepsins for execution [17], raising the possibility that HMA behaves analogously to lysosome-disrupting CADs that diffuse across cellular membranes, become protonated and trapped within the acidic lysosomal lumen, and exert their effects on lysosomal targets [42]. Indeed, we observed that HMA displaces

Preprints (www.preprints.org) | NOT PEER-REVIEWED | Posted: 6 January 2022 doi:10.20944/preprints202201.0082.v1

LysoTracker Red from lysosomal puncta in MDA-MB-231 and MCF7 cells (Figs. 6A and 6B), strongly supporting its lysosomal accumulation. Moreover, HMA-induced LMP induction was observed in both cell lines by complementary assays measuring the diffusion of pre-internalized fluorescent dextran from punctate lysosomes into the cytosol [24] (Figs. 6C-E) and the translocation of endogenous galectin from the cytosol to the inner membrane of lysosomes [20] (Figs 6F and 6G). In these experiments, HMA-induced LMP was detected prior to the onset of significant cell death (Supplementary Fig. S4A), and was as extensive as LMP induced by the previously described drugs siramesine and terfenadine [24]. Together, these findings point to a potential role for LMP in HMA mechanism of action.

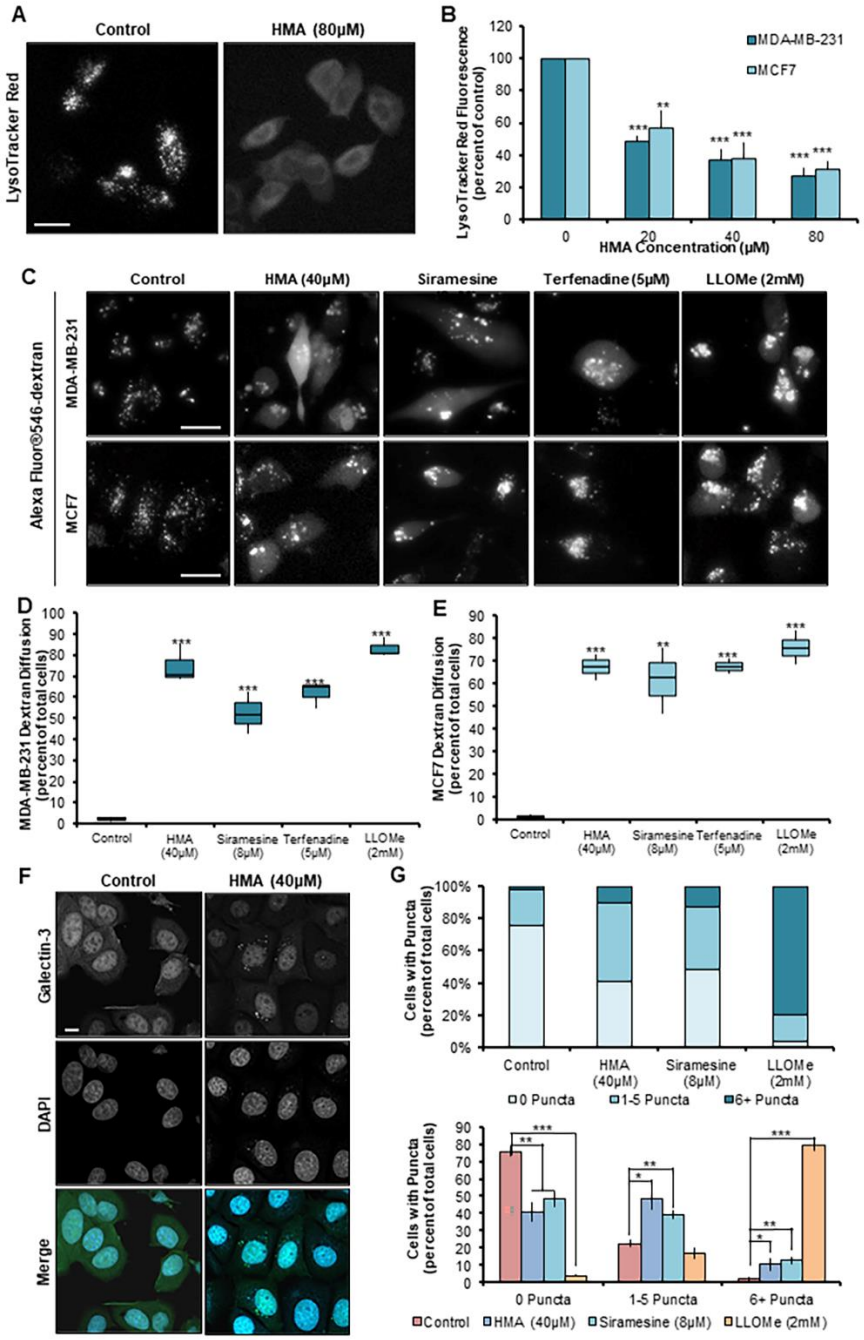

Figure 6. HMA induces lysosomal membrane permeabilization to kill breast cancer cells. (A,B) MDA-MB-231 and MCF7 cells were pretreated with 50nM LysoTracker Red for 30 minutes, and then treated with various concentrations of HMA. **(A)** Representative images of MCF7 LysoTracker Red fluorescence are displayed; scale bar = 20μm. **(B)** Fluorescence was quantified over three independent experiments for each cell line. **(C)** AlexaFluor 546-dextran-loaded MDA-MB-231 and MCF7

 doi:10.20944/preprints202201.0082.v1

cells were treated with vehicle, 40μM HMA, 8μM siramesine, 5μM terfenadine, or 2mM LLOMe for 20 hours; scale bar = 20μm. **(D,E)** The percentage of MDA-MB-231 **(D)** and MCF7 **(E)** cells exhibiting diffuse cytosolic Alexa Fluor 546-dextran staining was determined across three biological replicate experiments, with a minimum of 200 cells quantified for each replicate. Boxes represent the 2nd and 3rd quartiles, while whiskers extend to the maximum and minimum values. **(F,G)** MCF7 cells were treated with vehicle, 40μM HMA, 8μM siramesine or 2mM LLOMe for 12 hours, and stained for galectin-3. **(F)** Representative images are displayed; scale bar = 10μm. **(G)** The percentage of total cells with 0, 1-5, or 6+ galectin-3 puncta (presented as both distribution of puncta number, *top*, and percentage of total cells, *bottom*) were quantified across three biological replicates, and each replicate encompasses counts from 10 randomly selected fields. Error bars represent SEM. *, $P < 0.05$; **, $P < 0.01$; ***, $P < 0.001$, by Student's t-test.

4. Discussion

Collectively, our findings reveal the broad efficacy of HMA-induced LDCD and underscore the growing promise of lysosome-targeting therapeutic strategies in cancer treatment. We establish HMA as an LMP-inducing agent through application of highly sensitive assays for lysosome membrane rupture detection. While lysosome destabilizing compounds were evaluated as anti-cancer agents as early as the 1970s, the approach was temporarily abandoned due to a lack of specific methodology available to identify LMP as the causative event in cell death [20,63,64]. Meanwhile, the evolving study of lysosomal protease biology revealed diverse activities for cathepsins in cell death and disease. Pro-tumorigenic roles for cathepsins (promotion of cancer cell proliferation, invasion, and metastasis through extracellular matrix remodeling and stimulation of angiogenesis) have been established [26,65-67]; conversely, cathepsins function in LMP-mediated cell death mechanisms in cancer and other developmental and disease contexts [22,68,69]. Elevated cathepsin expression observed in malignant transformation, together with an expansion of the lysosomal compartment and alterations in membrane protein composition, serve to enhance tumor aggressiveness. However, these characteristic features of cancer cell lysosomes augment cellular susceptibility to LMP, providing strong rationale for lysosome-based therapeutic intervention [70].

Indeed, various agents that induce LMP or otherwise affect lysosomal function are under investigation for cancer, with few in clinical development, though clinical efficacy data is presently lacking for these strategies [70,71]. Preclinical evaluation of the CAD siramesine revealed its ability to induce LMP and tumor-selective cell death [21] hinging on displacement of the lipid-metabolizing enzyme acid sphingomyelinase (ASM) from its lipid cofactor bis(monoacylglycero)phosphate (BMP), thereby inhibiting hydrolysis of sphingomyelin to ceramide and disrupting membrane dynamics due to sphingomyelin accumulation [24]. Transformation-associated loss of ASM expression purportedly accounts for the cancer sensitization observed—accordingly, it will be prudent to identify HMA's lysosomal molecular target and uncover whether a similar mechanism underlies its tumor cell selectivity.

Moreover, current FDA-approved drugs with CAD-like properties including anti-histamines [72] and anti-malarials [73] display anti-tumor effects in preclinical as well as epidemiological studies. For example, a retrospective analysis of Danish patients diagnosed with ovarian cancer concluded that prior use of CAD anti-histamines was associated with a significant survival benefit [74]. Considering further the apparent safe long-term use of these clinical CADs—which exhibit lysosomotropic qualities including rapid organelle sequestration and phospholipidosis induction similar to HMA as demonstrated here and in our previous study [17]—as well as the decades-long clinical employment of amiloride and lack of non-specific HMA toxicity demonstrated *in vivo* and *in vitro* in these studies, it can be surmised that similar classes of LMP-inducing agents will be efficacious and well-tolerated as clinical development expands. Along these lines, a recent evaluation of the CAD anti-histamine clemastine reported LMP-mediated death of patient-derived glioblastoma cells but minimal cytotoxicity in normal human astrocytes [72], indicating a therapeutic window for treatment of this aggressive and lethal disease not unlike that observed in our HMA studies. Here, we have expanded on our previous observations that

 doi:10.20944/preprints202201.0082.v1

HMA selectively depletes transformed breast cancer cells by a lysosome-mediated mechanism, demonstrating HMA's ablation of glioblastoma cells relative to non-transformed murine brain cells as well as significant drug-induced cytotoxicity across bladder, colorectal, liver, lung, pancreatic, and prostate cancer cells. These findings are significant considering the lack of therapeutic options and poor survival outcomes for patients diagnosed with these diseases, particularly glioblastoma and cancers of lung, liver, and pancreatic origin [59-62].

Beyond demonstrating the broad spectrum of heterogeneous cancers sensitive to HMA's cytotoxicity, we established the translational relevance of our *in vitro* findings utilizing multiple *ex vivo* and *in vivo* models of breast cancer. We cultivated three-dimensional organoid systems to assess HMA's effects on tumor tissue viability, and further adopted a novel organotypic tumor slice culture technique to test drug response in tissues harvested from both genetically-modified and syngeneic orthotopic xenograft mouse models of mammary tumorigenesis. Importantly, unlike other cell and tissue culture systems, tumor slice cultures preserve the morphology and heterogeneity of the original tissue as well as an intact tumor microenvironment for extended periods [52]. We also found that intratumoral HMA administration induced necrotic cell death in Met-1 mammary xenograft tumors—consistent with our *in vitro* findings [17]—and reduced metastasis to the lung, which prompted us to evaluate the impact of systemically-delivered HMA/DCM-nanoparticles in an experimental metastasis model. HMA/DCM inhibited metastatic lung colonization and outgrowth, significant as CSCs exhibit enhanced survival in peripheral circulation and foreign tissue environments and are capable of differentiating and proliferating to form secondary tumors [75,76].

CSCs are critical drivers of tumor progression and metastasis and underlie key clinical challenges of recurrence and chemotherapy resistance, with increasing data demonstrating that CSCs can persist following targeted drug and immunotherapy administration. Critically, we found that HMA-induced LCD ablates heterogeneous tumor cell populations including chemotherapy insensitive "persister" cells and breast, brain, bladder, colorectal, liver, lung, pancreatic, and prostate CSCs alike. BCSCs isolated based on cell surface marker expression or functionally enriched by tumorsphere cultivation from molecularly diverse breast cancer subtypes and mouse-derived primary tumor cells were uniformly susceptible to HMA. This broad cytotoxicity is highly attractive, as addressing issues of inter- and intra-tumoral heterogeneity in cancer therapy design remains an enormous challenge, and many CSC-targeting agents in development rely on tissue-specific marker expression [77,78]. Despite pursuit of innovative solutions for CSC targeting including forced differentiation and CSC pathway inhibition, failure rates in clinical trials are high, with strategies largely limited by CSC plasticity and toxicity in normal stem cells [79]. Agents such as HMA and other CADs that subvert plasticity issues by effectively eliminating both total and CSC populations of heterogeneous tumor types offer tremendous potential in improving patient outcomes.

While few other studies have directly interrogated CSC cytotoxicity by lysosome-disrupting agents, a 2013 report showed co-expression of the lysosomal marker lysosome-associated membrane protein-1 (LAMP-1) with a marker of stemness in glioblastoma cells, indicating expansion of the lysosome compartment in CSCs [80]. Recently, the small molecule drug salinomycin was discovered to selectively kill CSCs through lysosomal iron sequestration, which catalyzed redox cycling and lysosomal ROS production, ultimately triggering LMP-mediated ferroptotic tumor cell death without displaying normal cell toxicity [81]. Together, these findings along with our observations of HMA's anti-CSC potency and transformation-selective effects support further investigation of lysosome-targeting drugs to meet the need for efficacious CSC-destroying agents. Potential applications of LMP inducers in clinical use are in fact wide-ranging, as CADs and other lysosome disrupting agents exhibit synergy with nanoparticles, proposed to enhance cellular internalization and targeting of existing anti-CSC compounds in development [79], by releasing them from sequestration in lysosomes [82]. Given transformation-associated changes

 doi:10.20944/preprints202201.0082.v1

to the lysosome compartment and mounting evidence that functional lysosomes contribute to multi-drug resistance, the lysosome is emerging as a compelling anti-cancer target.

5. Conclusions

When taken together with our previous observations, the current work demonstrates that HMA acts as efficiently toward therapy-resistant BCSC-like subpopulations as toward therapy-sensitive bulk breast cancer cell populations. These observations suggest that BCSC populations that are left intact by currently employed first-line chemotherapeutics may be sensitive to LMP-inducing agents. In this regard, CADs may be particularly useful as components of maintenance therapy regimens to eradicate residual CSCs following primary therapy, sidestepping synergistic toxicities of co-administered therapeutic agents. Moreover, cellular heterogeneity, plasticity and related issues that confound the development of CSC-targeting agents drop out of consideration with agents that exert their cytotoxic effects based on transformation-dependent vulnerabilities rather than cellular subtype-specific properties. Indeed, our observations suggest that the LMP induction approach may be applicable to a variety of malignancies. While the modest potency and poor pharmacokinetic properties of HMA preclude its development as an anti-neoplastic, CADs or even amiloride derivatives that act via a similar mechanism but with greater potency offer promise in thwarting recurrence and metastatic spread.

Supplementary Materials: The following supporting information can be downloaded at: www.mdpi.com/xxx/s1. Table S1: Characteristics of breast cancer cell lines; Table S2: Characteristics of non-mammary cancer cell lines; Figure S1: The BCSC subpopulation is susceptible to HMA-induced death; Figure S2: Chemoresistant cells are susceptible to HMA; Figure S3: Preparation and characterization of HMA-loaded DCM nanoparticles; Figure S4: LMP onset precedes significant cell death.

Author Contributions: Conceptualization, A.L.B., A.R.H. and K.L.C.; methodology, A.L.B., A.R.H. H.W., J.J., A.-M.Y., and Y.L.; formal analysis, A.L.B., A.R.H. and J.H.; investigation, M.H., M.K., K.V., J.J.C., C.A.D., and M.R.W.; resources, H.W., J.J., A.-M.Y., and Y.L.; writing—original draft preparation, A.L.B.; writing—review and editing, A.R.H., K.V., J.H., C.A.D., and K.L.C.; visualization, A.L.B.; supervision, A.-M.Y., Y.L., and K.L.C.; project administration, K.L.C.; funding acquisition, K.L.C. All authors have read and agreed to the published version of the manuscript.

Funding: These studies were supported by National Institutes of Health grants R01CA250211 and R01CA230742-S1 (KLC), T32GM099608 (AB), T32CA108459 (ARH), F31CA210467 (KV), F31CA165758 (JH), F31CA246900 (CD), R01CA253230 (AY), and R01DE029237 (YL).

Institutional Review Board Statement: The mouse studies were approved by the Institutional Animal Care and Use Committee of the University of California, Davis (protocol #21286, approved September 16, 2021).

Acknowledgments: We are grateful to Jonathan Van Dyke, Jane Chen and Catalina Simion for assistance with study design, methodology development and technical support, and to the UCD Comprehensive Cancer Center Flow Cytometry and Molecular Pharmacology Shared Resources supported in part by NIH grant P30CA093373.

Conflicts of Interest: A.M. Yu is the founder of AimRNA, Inc., a company that develops RNA technologies and therapeutics. The company had no role in the design of the study, in the collection, analyses, or interpretation of data, in the writing of the manuscript, or in the decision to publish the results. No potential conflicts of interest are disclosed by the other authors.

References

1. Al-Hajj M, Wicha MS, Benito-Hernandez A, Morrison SJ, Clarke MF. Prospective identification of tumorigenic breast cancer cells. Proc Natl Acad Sci USA. 2003; 100: 3983–3988.
2. Dalerba P, Dylla SJ, Park I-K, Liu R, Wang X, Cho RW, et al. Phenotypic characterization of human colorectal cancer stem cells. Proc Natl Acad Sci USA. 2007; 104: 10158–10163.
3. Li C, Heidt DG, Dalerba P, Burant CF, Zhang L, Adsay V, et al. Identification of pancreatic cancer stem cells. Cancer Res. 2007; 67: 1030–1037.

4. Stewart JM, Shaw PA, Gedye C, Bernardini MQ, Neel BG, Ailles LE. Phenotypic heterogeneity and instability of human ovarian tumor-initiating cells. Proc Natl Acad Sci USA. 2011; 108: 6468–6473.
5. Singh SK, Hawkins C, Clarke ID, Squire JA, Bayani J, Hide T, et al. Identification of human brain tumour initiating cells. Nature. 2004; 432: 396–401.
6. Dean M, Fojo T, Bates S. Tumour stem cells and drug resistance. Nat Rev Cancer. 2005; 5: 275–284.
7. Müller V, Stahmann N, Riethdorf S, Rau T, Zabel T, Goetz A, et al. Circulating tumor cells in breast cancer: correlation to bone marrow micrometastases, heterogeneous response to systemic therapy and low proliferative activity. Clin Cancer Res. 2005; 11: 3678–3685.
8. Gong C, Yao H, Liu Q, Chen J, Shi J, Su F, et al. Markers of tumor-initiating cells predict chemoresistance in breast cancer. PLoS One. 2010; 5: e15630.
9. Stenning SP, Parkinson MC, Fisher C, Mead GM, Cook PA, Fossa SD, et al. Postchemotherapy residual masses in germ cell tumor patients: content, clinical features, and prognosis. Medical Research Council Testicular Tumour Working Party. Cancer. 1998; 83: 1409–1419.
10. Masui K, Gini B, Wykosky J, Zanca C, Mischel PS, Furnari FB, et al. A tale of two approaches: complementary mechanisms of cytotoxic and targeted therapy resistance may inform next-generation cancer treatments. Carcinogenesis. 2013; 34: 725–738.
11. Hanahan D, Weinberg RA. Hallmarks of cancer: the next generation. Cell. 2011; 144: 646–674.
12. Ahmad A. Pathways to breast cancer recurrence. ISRN Oncol. 2013; 2013: 290568.
13. Longley DB, Johnston PG. Molecular mechanisms of drug resistance. J Pathol. 2005; 205: 275–292.
14. Breiden B, Sandhoff K. Emerging mechanisms of drug-induced phospholipidosis. Biol Chem. 2019; 401 :31–46.
15. Hu M, Carraway KL 3rd. Repurposing cationic amphiphilic drugs and derivatives to engage lysosomal cell death in cancer treatment. Front Oncol. 2020; 10:6 05361.
16. Ellegaard A-M, Bach P, Jäättelä M. Targeting cancer lysosomes with good old cationic amphiphilic drugs. Rev Physiol Biochem Pharmacol. Springer, Berlin, Heidelberg. 2021.
17. Rowson-Hodel AR, Berg AL, Wald JH, Hatakeyama J, VanderVorst K, Curiel DA, et al. Hexamethylene amiloride engages a novel reactive oxygen sp.ecies- and lysosome-dependent programmed necrotic mechanism to selectively target breast cancer cells. Cancer Lett. 2016; 375: 62–72.
18. Kittaneh M, Montero AJ, Glück S. Molecular profiling for breast cancer: a comprehensive review. Biomark Cancer. 2013; 5: 61–70.
19. Chan K-S, Koh C-G, Li H-Y. Mitosis-targeted anti-cancer therapies: where they stand. Cell Death Dis. 2012; 3: e411.
20. Aits S, Jäättelä M, Nylandsted J. Methods for the quantification of lysosomal membrane permeabilization: a hallmark of lysosomal cell death. Methods Cell Biol. 2015; 126: 261–285.
21. Ostenfeld MS, Fehrenbacher N, Høyer-Hansen M, Thomsen C, Farkas T, Jäättelä M. Effective tumor cell death by sigma-2 receptor ligand siramesine involves lysosomal leakage and oxidative stress. Cancer Res. 2005; 65: 8975–8983.
22. Aits S, Jäättelä M. Lysosomal cell death at a glance. J Cell Sci. 2013; 126: 1905–1912.
23. Fehrenbacher N, Gyrd-Hansen M, Poulsen B, Felbor U, Kallunki T, Boes M, et al. Sensitization to the lysosomal cell death pathway upon immortalization and transformation. Cancer Res. 2004; 64: 5301–5310.
24. Petersen NHT, Olsen OD, Groth-Pedersen L, Ellegaard A-M, Bilgin M, Redmer S, et al. Transformation-associated changes in sphingolipid metabolism sensitize cells to lysosomal cell death induced by inhibitors of acid sphingomyelinase. Cancer Cell. 2013; 24: 379–393.
25. Appelqvist H, Wäster P, Kågedal K, Öllinger K. The lysosome: from waste bag to potential therapeutic target. J Mol Cell Biol. 2013; 5: 214–226.
26. Kallunki T, Olsen OD, Jäättelä M. Cancer-associated lysosomal changes: friends or foes? Oncogene. 2013; 32: 1995–2004.
27. Miller JK, Shattuck DL, Ingalla EQ, Yen L, Borowsky AD, Young LJT, et al. Suppression of the negative regulator LRIG1 contributes to ErbB2 overexpression in breast cancer. Cancer Res. 2008; 68: 8286–8294.
28. Borowsky AD, Namba R, Young LJT, Hunter KW, Hodgson JG, Tepper CG, et al. Syngeneic mouse mammary carcinoma cell lines: two closely related cell lines with divergent metastatic behavior. Clin Exp Metastasis. 2005; 22: 47–59.
29. Cho RW, Wang X, Diehn M, Shedden K, Chen GY, Sherlock G, et al. Isolation and molecular characterization of cancer stem cells in MMTV-Wnt-1 murine breast tumors. Stem Cells. 2008; 26: 364–371.
30. Diehn M, Cho RW, Lobo NA, Kalisky T, Dorie MJ, Kulp AN, et al. Association of reactive oxygen species levels and radioresistance in cancer stem cells. Nature. 2009; 458: 780–783.
31. Siegel PM, Ryan ED, Cardiff RD, Muller WJ. Elevated expression of activated forms of Neu/ErbB-2 and ErbB-3 are involved in the induction of mammary tumors in transgenic mice: implications for human breast cancer. EMBO J. 1999; 18: 2149–2164.
32. Lee CY-F, Lin Y, Bratman SV, Feng W, Kuo AH, Scheeren FA, et al. Neuregulin autocrine signaling promotes self-renewal of breast tumor-initiating cells by triggering HER2/HER3 activation. Cancer Res. 2014; 74: 341–352.
33. Liu JC, Deng T, Lehal RS, Kim J, Zacksenhaus E. Identification of tumorsphere- and tumor-initiating cells in HER2/Neu-induced mammary tumors. Cancer Res. 2007; 67: 8671–8681.
34. Hangauer MJ, Viswanathan VS, Ryan MJ, Bole D, Eaton JK, Matov A, et al. Drug-tolerant persister cancer cells are vulnerable to GPX4 inhibition. Nature. 2017; 551: 247–250.
35. Sharma SV, Lee DY, Li B, Quinlan MP, Takahashi F, Maheswaran S, et al. A chromatin-mediated reversible drug-tolerant state in cancer cell subpopulations. Cell. 2010; 141: 69–80.

36. Nguyen-Ngoc K-V, Cheung KJ, Brenot A, Shamir ER, Gray RS, Hines WC, et al. ECM microenvironment regulates collective migration and local dissemination in normal and malignant mammary epithelium. Proc Natl Acad Sci USA. 2012; 109: E2595-2604.
37. Wu X, Roberto JB, Knupp A, Kenerson HL, Truong CD, Yuen SY, et al. Precision-cut human liver slice cultures as an immunological platform. J Immunol Methods. 2018; 455: 71–79.
38. Li Y, Xiao K, Luo J, Xiao W, Lee JS, Gonik AM, et al. Well-defined, reversible disulfide cross-linked micelles for on-demand paclitaxel delivery. Biomaterials. 2011; 32: 6633–6645.
39. Rowson-Hodel AR, Wald JH, Hatakeyama J, O'Neal WK, Stonebraker JR, VanderVorst K, et al. Membrane Mucin Muc4 promotes blood cell association with tumor cells and mediates efficient metastasis in a mouse model of breast cancer. Oncogene. 2018; 37: 197–207.
40. Yokdang N, Hatakeyama J, Wald JH, Simion C, Tellez JD, Chang DZ, et al. LRIG1 opposes epithelial-to-mesenchymal transition and inhibits invasion of basal-like breast cancer cells. Oncogene. 2016; 35: 2932–2947.
41. Rowson-Hodel AR, Manjarin R, Trott JF, Cardiff RD, Borowsky AD, Hovey RC. Neoplastic transformation of porcine mammary epithelial cells in vitro and tumor formation in vivo. BMC Cancer. 2015; 15: 562.
42. Kazmi F, Hensley T, Pope C, Funk RS, Loewen GJ, Buckley DB, et al. Lysosomal sequestration (trapping) of lipophilic amine (cationic amphiphilic) drugs in immortalized human hepatocytes (Fa2N-4 cells). Drug Metab Dispos. 2013; 41: 897–905.
43. Prat A, Parker JS, Karginova O, Fan C, Livasy C, Herschkowitz JI, et al. Phenotypic and molecular characterization of the claudin-low intrinsic subtype of breast cancer. Breast Cancer Res. 2010; 12: R68.
44. Dontu G, Abdallah WM, Foley JM, Jackson KW, Clarke MF, Kawamura MJ, et al. In vitro propagation and transcriptional profiling of human mammary stem/progenitor cells. Genes Dev. 2003; 17: 1253–1270.
45. Fillmore CM, Kuperwasser C. Human breast cancer cell lines contain stem-like cells that self-renew, give rise to phenotypically diverse progeny and survive chemotherapy. Breast Cancer Res. 2008; 10: R25.
46. Charafe-Jauffret E, Ginestier C, Iovino F, Wicinski J, Cervera N, Finetti P, et al. Breast cancer cell lines contain functional cancer stem cells with metastatic capacity and a distinct molecular signature. Cancer Res. 2009; 69: 1302–1313.
47. Diehn M, Cho RW, Clarke MF. Therapeutic implications of the cancer stem cell hypothesis. Semin Radiat Oncol. 2009; 19: 78–86.
48. Guy CT, Webster MA, Schaller M, Parsons TJ, Cardiff RD, Muller WJ. Expression of the neu protooncogene in the mammary epithelium of transgenic mice induces metastatic disease. Proc Natl Acad Sci USA. 1992; 89: 10578–10582.
49. Ingalla EQ, Miller JK, Wald JH, Workman HC, Kaur RP, Yen L, et al. Post-transcriptional mechanisms contribute to the suppression of the ErbB3 negative regulator protein Nrdp1 in mammary tumors. J Biol Chem. 2010; 285: 28691–28697.
50. Ramirez M, Rajaram S, Steininger RJ, Osipchuk D, Roth MA, Morinishi LS, et al. Diverse drug-resistance mechanisms can emerge from drug-tolerant cancer persister cells. Nat Commun. 2016; 7: 10690.
51. Lin EY, Jones JG, Li P, Zhu L, Whitney KD, Muller WJ, et al. Progression to malignancy in the polyoma middle T oncoprotein mouse breast cancer model provides a reliable model for human diseases. Am J Pathol. 2003; 163: 2113–2126.
52. Sivakumar R, Chan M, Shin JS, Nishida-Aoki N, Kenerson HL, Elemento O, et al. Organotypic tumor slice cultures provide a versatile platform for immuno-oncology and drug discovery. Oncoimmunology. 2019; 8: e1670019.
53. Lee C, Tannock I. Pharmacokinetic studies of amiloride and its analogs using reversed-phase high-performance liquid chromatography. J Chromatogr B Biomed Appl. 1996; 685: 151–157.
54. Luo J, Tannock IF. Inhibition of the regulation of intracellular pH: potential of 5-(N,N-hexamethylene) amiloride in tumour-selective therapy. Br J Cancer. 1994; 70: 617–624.
55. Alifieris C, Trafalis DT. Glioblastoma multiforme: Pathogenesis and treatment. Pharmacol Ther. 2015; 152: 63–82.
56. Bianco J, Bastiancich C, Jankovski A, des Rieux A, Préat V, Danhier F. On glioblastoma and the search for a cure: where do we stand? Cell Mol Life Sci. 2017;74: 2451–2466.
57. Lee C-H, Yu C-C, Wang B-Y, Chang W-W. Tumorsphere as an effective in vitro platform for screening anti-cancer stem cell drugs. Oncotarget. 2016; 7: 215–226.
58. Singh SK, Clarke ID, Terasaki M, Bonn VE, Hawkins C, Squire J, et al. Identification of a cancer stem cell in human brain tumors. Cancer Res. 2003; 63: 5821–5828.
59. Valtorta S, Lo Dico A, Raccagni I, Gaglio D, Belloli S, Politi LS, et al. Metformin and temozolomide, a synergic option to overcome resistance in glioblastoma multiforme models. Oncotarget. 2017; 8: 113090–113104.
60. Long J, Zhang Y, Yu X, Yang J, LeBrun DG, Chen C, et al. Overcoming drug resistance in pancreatic cancer. Expert Opin Ther Targets. 2011; 15: 817–828.
61. Lundholm L, Hååg P, Zong D, Juntti T, Mörk B, Lewensohn R, et al. Resistance to DNA-damaging treatment in non-small cell lung cancer tumor-initiating cells involves reduced DNA-PK/ATM activation and diminished cell cycle arrest. Cell Death Dis. 2013; 4: e478.
62. Marin JJG, Cives-Losada C, Asensio M, Lozano E, Briz O, Macias RIR. Mechanisms of Anticancer Drug Resistance in Hepatoblastoma. Cancers (Basel). 2019; 11:407.
63. Vanden Berghe T, Vanlangenakker N, Parthoens E, Deckers W, Devos M, Festjens N, et al. Necroptosis, necrosis and secondary necrosis converge on similar cellular disintegration features. Cell Death Differ. 2010; 17: 922–930.
64. Brunk UT, Ericsson JL. Cytochemical evidence for the leakage of acid phosphatase through ultrastructurally intact lysosomal membranes. Histochem J. 1972 Nov;4(6):479–91.
65. Gocheva V, Joyce JA. Cysteine cathepsins and the cutting edge of cancer invasion. Cell Cycle. 2007; 6: 60–64.

66. Benes P, Vetvicka V, Fusek M. Cathepsin D--many functions of one aspartic protease. Crit Rev Oncol Hematol. 2008; 68: 12–28.
67. Gocheva V, Wang H-W, Gadea BB, Shree T, Hunter KE, Garfall AL, et al. IL-4 induces cathepsin protease activity in tumor-associated macrophages to promote cancer growth and invasion. Genes Dev. 2010; 24: 241–255.
68. Kirkegaard T, Jäättelä M. Lysosomal involvement in cell death and cancer. Biochim Biophys Acta. 2009; 1793: 746–754.
69. Pišlar A, Perišić Nanut M, Kos J. Lysosomal cysteine peptidases - Molecules signaling tumor cell death and survival. Semin Cancer Biol. 2015; 35: 168–179.
70. Davidson SM, Vander Heiden MG. Critical Functions of the Lysosome in Cancer Biology. Annu Rev Pharmacol Toxicol. 2017; 57: 481–507.
71. Bonam SR, Wang F, Muller S. Lysosomes as a therapeutic target. Nat Rev Drug Discov. 2019; 18: 923–948.
72. Le Joncour V, Filppu P, Hyvönen M, Holopainen M, Turunen SP, Sihto H, et al. Vulnerability of invasive glioblastoma cells to lysosomal membrane destabilization. EMBO Mol Med. 2019; 11: e9034.
73. Das S, Dielschneider R, Chanas-LaRue A, Johnston JB, Gibson SB. Antimalarial drugs trigger lysosome-mediated cell death in chronic lymphocytic leukemia (CLL) cells. Leuk Res. 2018; 70: 79–86.
74. Verdoodt F, Dehlendorff C, Jäättelä M, Strauss R, Pottegård A, Hallas J, et al. Antihistamines and Ovarian Cancer Survival: Nationwide Cohort Study and in Vitro Cell Viability Assay. J Natl Cancer Inst. 2020; 112: 964–967.
75. Lawson DA, Bhakta NR, Kessenbrock K, Prummel KD, Yu Y, Takai K, et al. Single-cell analysis reveals a stem-cell program in human metastatic breast cancer cells. Nature. 2015; 526: 131–135.
76. Baccelli I, Trumpp A. The evolving concept of cancer and metastasis stem cells. J Cell Biol. 2012; 198: 281–293.
77. Turdo A, Veschi V, Gaggianesi M, Chinnici A, Bianca P, Todaro M, et al. Meeting the Challenge of Targeting Cancer Stem Cells. Front Cell Dev Biol. 2019; 7: 16.
78. Marquardt S, Solanki M, Spitschak A, Vera J, Pützer BM. Emerging functional markers for cancer stem cell-based therapies: Understanding signaling networks for targeting metastasis. Semin Cancer Biol. 2018; 53: 90–109.
79. Batlle E, Clevers H. Cancer stem cells revisited. Nat Med. 2017; 23: 1124–1134.
80. Jensen SS, Aaberg-Jessen C, Christensen KG, Kristensen B. Expression of the lysosomal-associated membrane protein-1 (LAMP-1) in astrocytomas. Int J Clin Exp Pathol. 2013; 6: 1294–1305.
81. Mai TT, Hamaï A, Hienzsch A, Cañeque T, Müller S, Wicinski J, et al. Salinomycin kills cancer stem cells by sequestering iron in lysosomes. Nat Chem. 2017; 9: 1025–1033.
82. Du Rietz H, Hedlund H, Wilhelmson S, Nordenfelt P, Wittrup A. Imaging small molecule-induced endosomal escape of siRNA. Nat Commun. 2020; 11: 1809.